International Journal of Nanoelectronics and Materials
IJNeaM
ISSN 1985-5761 | E-ISSN 2232-1535

Single Step Formation Of Gold Core -Niobium Pentoxide Shell Nanoparticles Using Laser Ablation Technique: Effect of Laser Pulse Number

Mohammed Moslih Mahdi[a,c,*], Evan T. Salim[b,*], Ahmed S. Obaid[a]

[a]*Department of Physics, College of Science, University of Anbar, Anbar, Iraq*
[b]*Applied science department, University of Technology- Iraq, Baghdad, Iraq*
[c]*Department of Physics, College of Education for Pure Science, University of Anbar, Iraq*
**Corresponding author. Tel.: h/p: +9647715752087; e-mail: mohammed.moslih@uoanbar.edu.iq ,evan.t.salim@uotechnology.edu.iq*

ABSTRACT

Plasmonic nanoparticles improve light absorption and enhance the charge carrier lifetime of the semiconductor, which provides a tremendous contribution to the advanced field. UV-VIS study indicates the modification of band gap energy and visual absorption with the contrast of the particles in the Nb_2O_5 nanoparticles resulting from changing the number of laser pulses (from 3.25 to 2.71eV). XRD analyses revealed the successful casing of core-shell (Au) in the Nb_2O_5 nanoparticle by showing gold vulgar planes in (041) and (111) between Nb_2O_5. TEM images showed morphological changes and average size modification from 38.18 to 118.1 nm with the size variation of Au@Nb_2O_5 nanoparticles. Also, it confirmed the successful formation of core-shell nanoparticles. AFM images showed a directional proportion of the surface roughness rate with the number of laser pulses. The electrical resistance showed obvious improvement and decrease in value with the increasing number of laser pulses.

KeyWord: *Core@shell, Nanoparticles, Au@Nb_2O_5, Electrical properties, Laser Ablation in liquid, Hybrid structure*

1. INTRODUCTION

Integrating metallic NPs such as gold, with other types in designing hybrid nanoparticles provides a great opportunity in materials chemistry for different physical or chemical functions. The reciprocal interactions (electronic, structural, etc.) between the two components of the nanostructure may result in the formation of unique functions. This is due to the synergistic effects that transcend the simple amalgamation of the physico-chemical properties of the two components. Core-shell nanocomposites have received wide attention due to their unique physical, chemical, and biological properties, as well as their exceptional catalytic applications [1-3]. The thickness of the outer layer plays a vital role in determining the efficiency and performance of these nanocomposites. For example, in Surface-enhanced Raman scattering (SERS) applications based on noble metal nanoparticles encased in specialized shells, the thickness of the outer layer should be in the nanometer range. If the shell is too thick, it may significantly reduce or even eliminate the SERS signal intensity. This is negatively affecting the detection efficiency of target molecules [4, 5].

Niobium pentoxide (Nb_2O_5) is a metal oxide with significant promise yet to be thoroughly exploited. The interest in Nb_2O_5 originated in the early 1940s when its polymorphs were initially examined [6]. Nb_2O_5 exhibits numerous polymorphic forms, resulting in a compelling array of structural phases. These phases are predominantly derived from NbO6 octahedral groups, which assemble into diverse configurations, including rectangular blocks or columns [7, 8]. Nonetheless, most of these studies remain nascent, necessitating further research to ascertain the potential of Nb_2O_5 in these and additional applications. Consequently, more extensive investigations on Nb_2O_5 are necessary to furnish additional insights for researchers planning to utilize this material for such applications [9].

Laser ablation of metal targets in liquids represents an innovative and efficient technique for producing core@shell nanomaterials in a single step [10-12]. This method provides a flexible and environmentally sustainable option for the fabrication of metal nanoparticles, including elements such as gold, silver, platinum, and nickel. The resulting particles exhibit unique properties, such as high chemical activity, limited structural stability, and distinct surface modifiability, along with high purity and uniform distribution, making them ideal for applications in catalysis and surface-enhanced Raman scattering (SERS) research [13]. Kautek et al. synthesized Ni/NiOx core/shell nanoparticles in aqueous and alcoholic solutions, with the fluid type, laser fluence, and pulse count determining the size distribution of the resultant products. The alteration of these factors modified the size distribution of Ni/NiOx core/shell nanoparticles from 10 to 30 nm [14].

In 2019, Halboos and Salim synthesized Nb_2O_5 nanostructures by using a drop-casting approach. The produced Nb_2O_5 nanostructures were adorned with silver (Ag) nanoparticles through immersion in $AgNO_3$ solution for varying durations (30 to 120 seconds), followed by photo-activation via UV irradiation. The authors intended to construct a pn-heterojunction device. Nb_2O_5@Ag/Si exhibited superior performance relative to the Nb_2O_5/Si

manufactured device [15, 16]. Recently, Nogueira et al. (2020) functionalized Nb_2O_5 with CuO by a solvothermal treatment method. The work aimed to improve the photocatalytic activity of Nb_2O_5 adorned with CdO quantum dots for ambient carbon dioxide, yielding satisfactory results [17]. In addition, Ahmed et al. functionalized ZnO nanostructures with gold (Au) nanoparticles to examine the photocatalytic efficacy of the ZnO@Au heterostructure against Rhodamine B. The preparation method employed was green synthesis, utilizing pecan nut leaves as reducing agents, which led to effective ZnO@Au photocatalytic activity [18].

In this work, we investigated the influence of the number of pulse lasers on the productivity of Au@Nb_2O_5 core-shell nanoparticles during nanosecond laser ablation of bulk niobium immersed in gold colloidal. To our knowledge, the impact of the number of pulse parameters on the optical, structural, morphological, and electrical properties of core-shell nanoparticles in a dual-step process has not been thoroughly investigated.

2. EXPERIMENTAL WORK

Gold (Au) was initially generated by ablating a high-purity gold (99%) target submerged in pure doubly distilled water using an Nd: YAG laser. The operating factors were set at 1064 nm, with a pulse duration of 7 ns, a frequency of 1 Hz, and a spot size of approximately 0.8 mm; applying a fluence of 76.4 J/cm^2 over 400 laser pulses. The second phase involves positioning a niobium metal target at the base of a glass vessel, submerged in 3 mL of gold colloid, subjected to a fluence of 127.3 J/cm^2, at a wavelength of 1064 nm, with varying pulse counts (200, 300, 400, 500, 600). The experimental setup is illustrated in Figure 1.

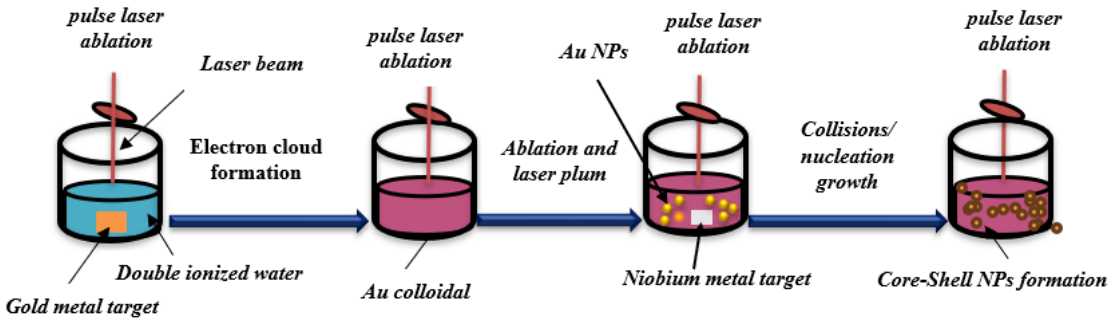

Figure 1. The steps of preparation Au@Nb_2O_5 core-shell NPs.

Quartz glass substrates and silicon substrates were supplied by China National Machinery Company, China. The substrates were purified by submerging in distilled water in a glass container, which was then placed in an ultrasonic bath for 15 minutes. Subsequently, they were immersed in methanol alcohol. The process was repeated three times before drying the substrates. Following the cleaning and drying of the glass substrates, a chemical spray pyrolysis method was employed to deposit the thin films. The substrates were positioned on the electric heater's surface for 10 minutes before the deposition process to ensure attaining the surface the required temperature. Upon affixing the spray apparatus to the metallic holder and calibrating the distance between the spray apparatus's nozzle and the substrates to approximately 29 cm, the solution of the substance intended for deposition is thereafter introduced into the spray apparatus reservoir. The volume of the flowing solution is regulated via a valve in the spray apparatus to achieve the desired spray rate of 2 ml/min. The spray duration is regulated by an electronic timer, set to 5 seconds for spraying and 20 seconds for cessation, allowing the base temperature to revert to the requisite level, which diminishes due to the quick cooling from the spray application.

3. RESULT AND DISCUSSION

3.1 UV-VIS Analysis

In plasmonic nanoparticles, such as Au@Nb_2O_5, the number of laser pulses can affect the plasmonic resonance properties by altering the shell thickness and uniformity. This is crucial for applications in sensing and photothermal therapies. The optical characteristics of synthetic Au@Nb_2O_5 core-shell nanoparticles were investigated by varying numbers of laser pulses and examined using UV-VIS spectroscopy. Figure 2 illustrates the absorption spectrum of five produced Au@Nb_2O_5 core-shell nanoparticle samples (200, 300, 400, 500, 600) pulses. The inter band absorption spectrum of the Nb_2O_5 shell displays a hump-like absorption peak at around 355 nm. The absorption peaks experience a red shift as the thickness of the Nb_2O_5 shell increases. The absorption peak of Nb_2O_5 nanoparticles resulted from the interaction between valence band electrons and incoming photons, leading to the excitation of these electrons to the conduction band. For Au nanoparticles, which are metallic, the pronounced absorption peak arises from the surface plasmon resonance of electrons within the conduction band [19, 20].

All the spectra display identical characteristics. The absorption spectra in the visible spectrum region are primarily characterized by the broad interband absorption band of Nb_2O_5, lacking any distinct excitonic absorption peak. The spectra display a distinct and extensive SPR peak of the Au nanocores around 530 nm. Typically, Au nanospheres exhibit a singular absorption band within the visible spectrum. The absorbance increased with a little red shift that was attributed to the augmented quantity of Nb_2O_5 nanoparticles in the suspension. This resulted from the greater volume of ablated material, which led to a higher concentration of Nb_2O_5 nanoparticles [21].

The UV-Vis spectra of Au@Nb_2O_5 core/shell nanoparticles demonstrate a considerable increase in the intensity of the Nb_2O_5 absorption peak as the number of laser pulses increases. The heightened absorption intensity of Nb_2O_5 can be attributed to the screening effect of the Nb_2O_5 shell surrounding the Au particles. Consequently, a substantial quantity of absorbable photons can be efficiently collected by the Nb_2O_5 shell [22].

Ultimately, as anticipated, each sample exhibits two absorption peaks associated with the nanoparticles. The spectra indicate the formation of Au@Nb_2O_5 core/shell nanoparticles in the colloidal medium. The two absorption peaks of Au@Nb_2O_5 core/shell nanocomposites do not merely represent a straightforward superposition of their components. These findings align with [23, 24].

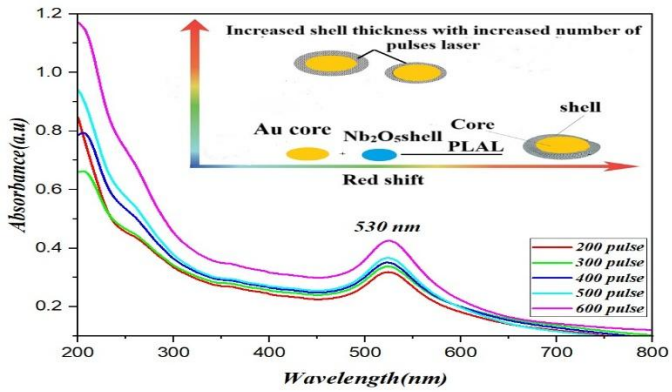

Figure 2. Illustrates the absorbance spectra of Au@Nb_2O_5 nanoparticles that were synthesized using varying pulses laser.

Au@Nb_2O_5 was synthesized with a Nd:YAG pulsed laser with a wavelength of 1064 nm and an optimal laser fluence of 127.3 J/cm^2. The optical band gaps and transmission spectra for each prepared sample, corresponding to varying numbers of laser pulses, are presented in Table 1. The indirect band gaps were calculated using Equation (1) [25-27].

$$\alpha h\mu = A\left(hv - E_{op}\right)^{1/2} \quad (1)$$

Where α absorption coefficient (cm^{-1}), hν photon energy (eV). E g: band gap (eV). The band gap of the synthesized thin films was determined by extrapolating the linear portion of the $(\alpha h\nu)^{0.5}$–hν graph concerning the incoming photon energy (3.25, 3.15, 2.95, 2.83, and 2.71) eV, respectively. The band gap reduced as the number of laser pulses increased due to the increase in particle size [28]. The correlation between the band gap energy Eg and the thickness of the Nb_2O_5 shell is illustrated in Figure 3. Furthermore, an increase in the thickness of the Nb_2O_5 shell leads to a greater band gap energy (Eg). The notable alteration in the band gap energy Eg and the transition of absorption peaks from band to band for the manufactured Nb_2O_5 shell on the gold nano core can be ascribed to the quantum confinement effect of the Nb_2O_5 shell [29].

The findings indicated that the band gap values diminished with an increased number of laser shots, reaching up to 300. A redshift was noted with an increasing number of laser pulses. This is due to the consistent rotation of the target. The produced particles may occupy identical precise positions in the colloidal solution previously occupied by the initial particles, leading to the formation of bigger species which is aligned with [30, 31].

Nb_2O_5 is an n-type semiconductor characterized by a wide band gap and a conduction band consisting of vacant Nb^{5+} 4d orbitals. Thus, the integration of an Au core with an Nb_2O_5 shell would explain the intermediate band gap value of 2.71 eV seen with a 600-pulse laser. The results indicated that these materials should enable the generation of electron-hole pairs and hydroxyl radicals, hence positioning them as possible photocatalysts for optoelectronic applications and cost reduction in processes [32].

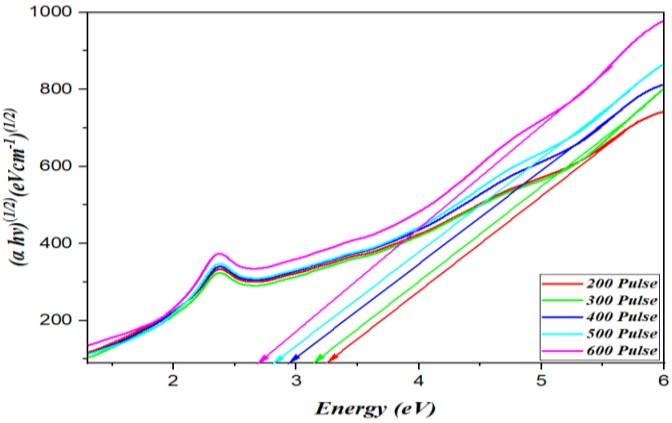

Figure 3. The Energy gap and absorption spectra of Au@Nb_2O_5 with different quantities of laser pulses.

Table 1 The indirect band gap of Au@Nb_2O_5 NPs produced with varying numbers of laser pulses.

Quantity of Laser Pulses	Indirect Bandgap in (eV)
200	3.25
300	3.15
400	2.95
500	2.83
600	2.71

3.2 X-ray Diffraction (XRD)

The XRD was employed to study the structure of Au@Nb_2O_5 that was prepared by different laser pulses (200, 300, 400, 500, 600, and 700) at a fluence energy of 127.3 J/cm^2 and a wavelength of 1064 nm. Figure 4 illustrates the distinct diffraction peaks for the orthorhombic T-Nb_2O_5 phase, aligned with JCPDS (card number 00-030-0873). The diffraction peaks are observed at 2θ = 25.7°, 64.8°, and 77.5°, which correspond to the orientations (041), (671), and (3122), respectively. The diffraction peak for monoclinic H-Nb_2O_5 was located at 2θ = 58.8° with the orientation (004) indexed by JCPDS (card number 00-027-1312). The peak with diffraction angles 2θ = 83.7° corresponds to the pure cubic phase of niobium, corresponding with JCPDS card number 00-034-0370.These findings align with [33-36]. More intense peaks emerged with a greater number of laser pulses employed in the preparation of Nb_2O_5. This phenomenon can be ascribed to the formation of additional particles exhibiting enhanced crystallinity [37].

Conversely, the sample subjected to 700 laser shots exhibited an extra peak at 2θ =82°, corresponding to the (215) plane, which is associated with the oxidation state of NbO_2 (tetragonal), corresponding with JCPDs (01-071-0020). The intensity of further peaks is also noted to diminish. This may signify the deterioration of the Nb_2O_5 crystal structures and alterations in the favored orientations of these structures may transpire. Additionally, it can be asserted that the PLAL technique involves regular rotation of the target, resulting in increased thermal shock waves being generated on the same regions of the rotating target surface due to the greater number of laser pulses employed in the ablation process.

The diffraction peaks at 2θ = 38.1°, 44.3°, and 64.5° correspond to the (111), (2 0 0), and (220) planes of the cubic crystal structure of the Au nanoparticles, which is in good accord with JCPDS card number 00-004-0784. The intensity of the primary diffraction peak of Au (111) nanostructures diminished relative to the diffraction peak of Nb_2O_5(041), which exhibited a pronounced increase with the rising number of pulses. This may come from the elevated quantities of clustered and agglomerated Nb_2O_5 nanoparticles.

With the increasing number of laser pulses, more pronounced peaks of the orthorhombic (T-Nb_2O_5) and monoclinic (H-Nb_2O_5) structures emerged. This can be explained by the increased amount of particles generated as a result of enhanced crystallinity. Each laser pulse contributes to the removal of a specific amount of target material, leading to improved nanoparticle production and better crystallinity [38]. The data demonstrated that the use of 600 laser pulses produced the highest and most intense peaks of Nb_2O_5 nanoparticles, indicating excellent crystallization of the material, while also revealing a peak associated with pure Niobium nanoparticles. The appearance of the diffraction planes for both Nb_2O_5 and Au signifies the heterogeneous structure of Au@Nb_2O_5. The formation of the core-shell structure reduced the Au diffraction peak. Moreover, the dimensions of the core and the shell's thickness may substantially affect the quality of crystallinity when exposed to laser pulses.

Finally, the intensity of the noble metal (Au) peaks progressively diminished for all the aforementioned laser pulses. This behavior can be ascribed to the protection of the noble metal (Au) core by Nb_2O_5 shells. Analogous conduct was noted [39, 40].

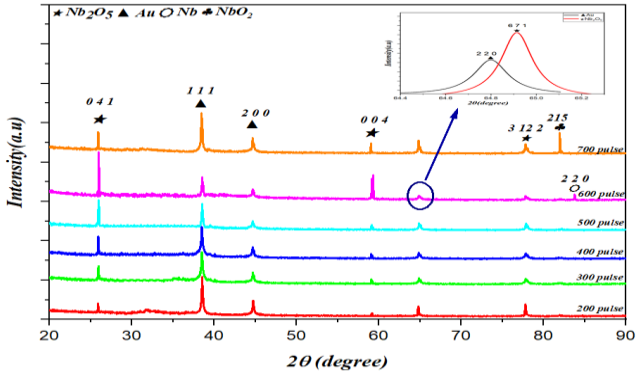

Figure 4. XRD patterns of Au@Nb_2O_5 core-shell prepared by a various number of pulses laser.

The values of Miller indices (hkl), crystallite size (D), crystalline defect density (δ), full width at half maximum (β), and microstrain (ε) of Au@Nb_2O_5 prepared at different pulses laser are shown in Table 2. The full half-width maximum (FWHM) is used to evaluate the amplitude of the peaks at the midpoint of their maximum intensity [41]. The average crystal grain size (D) is calculated using the Scherrer equation(Eq2), which allows estimating the crystallite size based on the width of the peaks and their value at half maximum[42-44]:

$$D_{XRD}=\frac{0.9\lambda}{\beta Cos\theta} \quad (2)$$

Where β represents the FWHM.

The application of a greater number of laser pulses increased the size of the crystallite. As a result, both the dislocation density and microstrain (δ) showed a decrease, signifying an enhancement in the quality of the resulting thin film.

Table 2 lists various parameters calculated based on the above equations including the crystalline size, the Miller indices, dislocation density, and the macrostrains of the Au@Nb_2O_5 core-shell material.

Table 2 The FWHM, crystal size, dislocation density, Miller indices, and macrostrains of the Au@Nb_2O_5 NPs

Number of pulses laser	2θ	FWHM	Miller indices	Crystalline size(nm)	Dislocation density(δ) x10^{-3}	Micro strains (nm^{-2}) x10^{-3}	Crystal system	Chemical formula	Card No. (JCPDS)
200	25.7°	0.413	0 4 1	19.8	2.52	7.77	T- Nb_2O_5	Nb_2O_5	00-030-0873
	58.8°	0.06	0 0 4	133.70	0.55	5.28	H- Nb_2O_5	Nb_2O_5	00-027-1312
	64.7°	0.25	6 7 1	36.44	7.53	17.75	T- Nb_2O_5	Nb_2O_5	00-030-0873
	77.5°	0.11	3122	94.03	1.13	5.62	T- Nb_2O_5	Nb_2O_5	00-030-0873
300	25.7°	0.328	0 4 1	24.85	1.61	6.21	T- Nb_2O_5	Nb_2O_5	00-030-0873
	58.8°	0.07	0 0 4	125.77	0.63	5.61	H- Nb_2O_5	Nb_2O_5	00-027-1312
	64.7°	0.15	6 7 1	61.09	2.61	10.58	T- Nb_2O_5	Nb_2O_5	00-030-0873
	77.5°	0.24	3122	43.84	5.20	12.05	T- Nb_2O_5	Nb_2O_5	00-030-0873
400	25.7°	0.322	0 4 1	25.31	1.56	6.11	T- Nb_2O_5	Nb_2O_5	00-030-0873
	58.8°	0.8407	0 0 4	10.84	8.500	65.10	H- Nb_2O_5	Nb_2O_5	00-027-1312
	64.7°	0.2817	6 7 1	33.40	8.96	19.36	T- Nb_2O_5	Nb_2O_5	00-030-0873
	77.5°	0.8407	3122	12.51	63.82	42.22	T- Nb_2O_5	Nb_2O_5	00-030-0873

500	25.9°	0.243	0 4 1`	33.55	0.88	4.59	T- Nb_2O_5	Nb_2O_5	01-074-1646
	58.8°	0.077	0 0 4	118.11	0.71	5.97	H- Nb_2O_5	Nb_2O_5	00-027-1312
	64.7°	0.15	6 7 1	61.45	2.64	10.52	T- Nb_2O_5	Nb_2O_5	00-030-0873
	77.5°	0.091	3122	115.43	0.75	4.57	T- Nb_2O_5	Nb_2O_5	00-030-0873
600	25.7°	0.186	0 4 1	43.83	0.52	3.51	T- Nb_2O_5	Nb_2O_5	00-030-0873
	58.8°	0.067	0 0 4	135.49	0.54	5.21	H- Nb_2O_5	Nb_2O_5	00-027-1312
	64.7°	0.095	6 7 1	99.04	1.01	6.53	T- Nb_2O_5	Nb_2O_5	00-030-0873
	77.5°	0.33	3122	34.02	0.86	1.62	T- Nb_2O_5	Nb_2O_5	00-030-0873
	83.7°	0.088	2 2 0	118.6	0.709	4.45	Cubic	Nb	00-034-0370
700	25.7°	0.21	0 4 1	38.8	0.66	3.97	T- Nb_2O_5	Nb_2O_5	01-074-1646
	58.8°	0.079	0 0 4	115.42	0.075	0.61	H- Nb_2O_5	Nb_2O_5	00-027-1312
	64.7°	0.5	6 7 1	18.8	2.827	3.44	T- Nb_2O_5	Nb_2O_5	00-030-0873
	77.5°	0.33	3122	34.02	0.86	1.62	T- Nb_2O_5	Nb_2O_5	00-030-0873
	82°	0.106	215	99.22	0.101	0.533	Tetragonal	NbO_2	01-076-1095

Figure 5 demonstrates that lattice strain decreases progressively with an increase in the number of laser pulses, leading to a concomitant increase in both the concentration and size of the particles. The produced nanoparticles display diverse sizes and oxide shell thicknesses, dependent on the dimensions of the nanoparticle core and the shell thickness. Varying nanoparticle sizes induce distinct lattice stresses within the core. The micro-strain was established by assessing the lattice parameters and micro-strain of the lattice in relation to the nanoparticle core's crystal size and shell thickness. Augmenting the particle size results in a reduction in micro-strain within the crystal lattice of the core. This is attributed to the elevated stress ratio at the core-shell contact relative to the entire core volume in smaller nanoparticles [45].

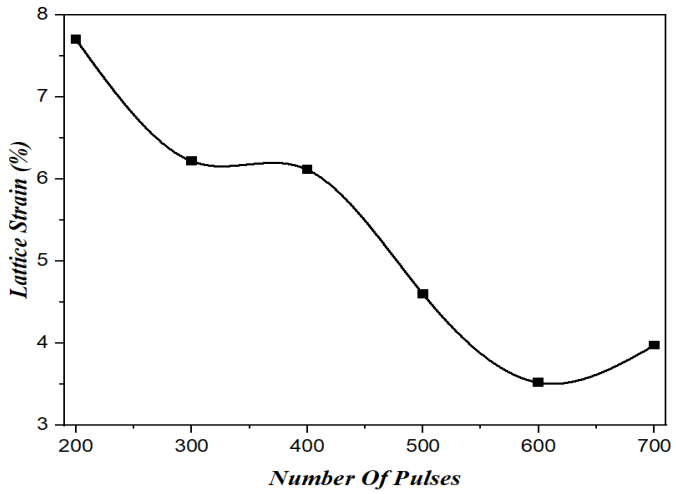

Figure 5. The variation of lattice strain (%) of Au@Nb_2O_5 as a function of laser pulses.

3.3 Atomic Force Microscopy (AFM)

Figure 6 displays high-magnification topographical views of the surface, accompanied by average-size histograms of $Au@Nb_2O_5$ nanoparticles generated with a laser fluence of 127.3 J/cm^2 with varying laser pulses. The table3 shows the values of the average particle size, roughness, and root mean square of $Au@Nb_2O_5$ nanoparticles.

The average particle size changes with laser pulses, these results are consistent with [46]. The data indicate that the particles are oriented vertically with various shapes. The average particle size was observed to increase with the increasing number of laser pulses (ranging from 44 to 78 nm). This change can be attributed to the increase in surface roughness of the nanoparticles, as shown in the previous observations.[47, 48]. The surface roughness and roughness root mean square increased with the number of laser pulses, corroborating other reported studies [49]. The AFM results are consistent with the findings from TEM, and XRD presented in this study.

The intensity of the thermal shock waves increases with each interaction between the laser beam and the target material at each pulse. The subsequent pulse may contribute to the ejection of species, which contributes to the overall improvement of the ablation process. For $Au@Nb_2O_5$ thin films, it was observed that the surface roughness increased with the increasing number of pulses. These results are consistent with previous studies. Increasing the number of laser pulses to 600 pulses decreases the surface roughness, which can be attributed to the improvement in homogeneity and the increase in particle size [39].

TEM imaging indicates that the heterojunctions obtain a good contact interface, which is beneficial for photoelectric performance. The better symmetry and reduction of roughness in $Au@Nb_2O_5$ films help to enhance the mobility of photogenerated charge carriers and inhibit charge recombination.

The $Au@Nb_2O_5$ prepared with 600 pulses exhibited uniformity compared to other surface coatings. The coated sample with minimal surface roughness experiences reduced scattering of incident light, resulting in enhanced light transmittance [50]. This facilitates optimal performance of the optoelectronic device. The roughness of the thin film correlates with the crystal size determined by the Scherrer equation based on XRD patterns, indicating that a smoother surface is associated with larger crystal sizes [51, 52]. Furthermore, given the significant impact of thin film roughness on photodetector performance, it is anticipated that a high-response photodetector can be developed using $Au@Nb_2O_5$.

Table 3. The surface roughness, average particle size, and root mean square of $Au@Nb_2O_5$ NPs.

Number of Laser pulses	Average particle Size (nm)	Roughness (nm)	Root mean square(nm)
200	± 44	2.337	4.38
300	± 51	3.01	82.3
400	± 58	3.74	89.19
500	± 63	4.99	64.08
600	± 78	4.37	10.01

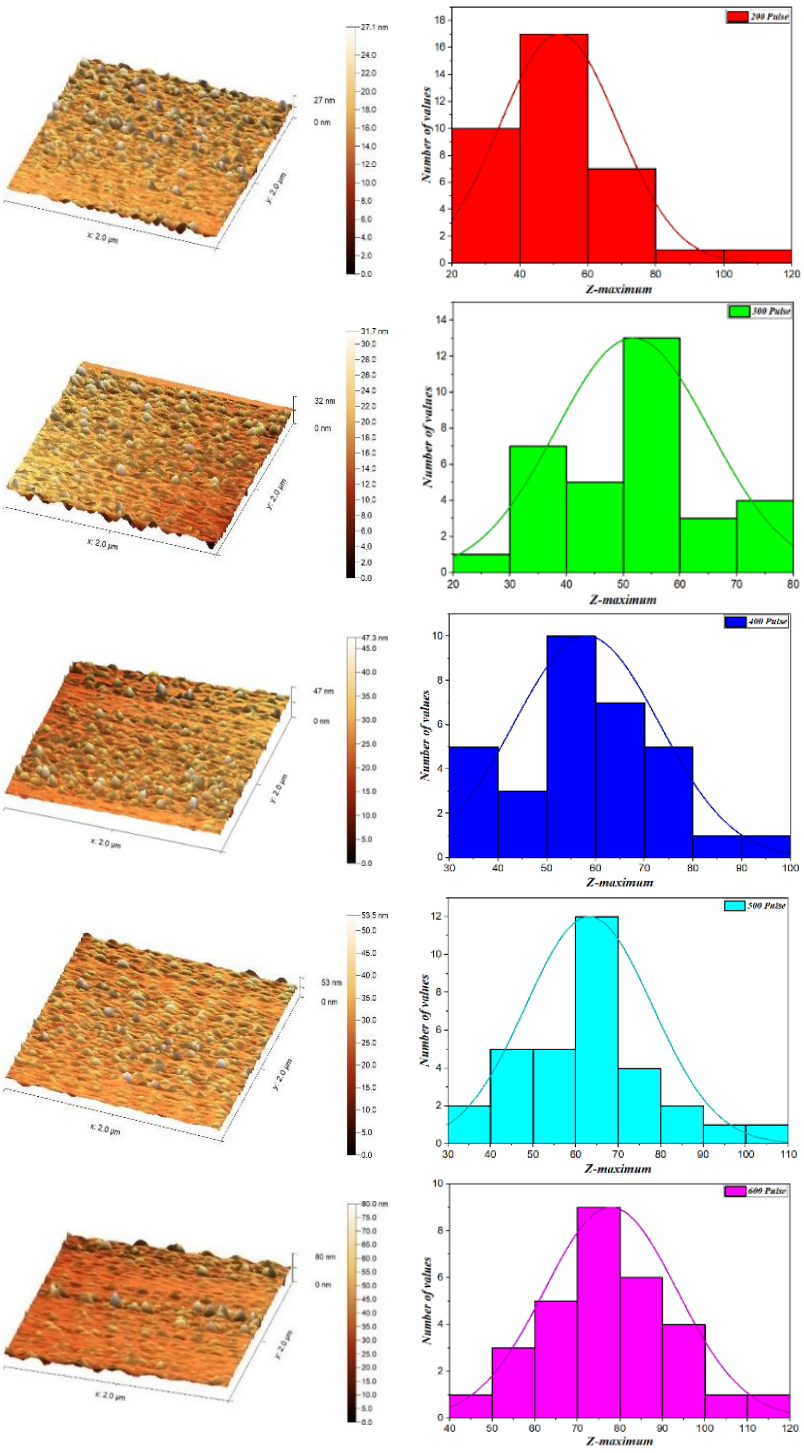

Figure 6. AFM images and histograms distribution of Au@Nb_2O_5 NPs.

3.4 Transmission Electron Microscopy (TEM)

The number of laser pulses during laser ablation in liquid (LAL) plays a crucial role in the formation and characteristics of core-shell nanoparticles. This technique involves using laser pulses to ablate a target material in a liquid medium, leading to the formation of nanoparticles.

Figure 7 shows TEM images of Au@Nb_2O_5 nanoparticles fabricated by 1064 nm wavelength of Nd:YAG laser and 127.3 J/cm^2 with a range of laser pulses (200-600). TEM images indicate that the NPs are interconnected spherical and are composed of black core (Au) and grey shell (Nb_2O_5). Interconnecting of NPs can have different reasons [53, 54]. In the beginning, a small number of laser pulses primarily contributes to the nucleation of core nanoparticles. These pulses generate a high concentration of ions and atoms from the target material, which then nucleate to form initial core nanoparticles. Generally, the nanoparticles showed a well-defined spherical shape that agglomerated within the concentration. The sample prepared with 200 laser shots showed a low concentration of Nb_2O_5 nanoparticles with low shell thickness (5.12 nm) and agglomeration rate. This number of laser pulses was not sufficient to dislodge enough

amount of material. As the number of pulses increases, more material is ablated and added to the solution. This additional material can be deposited on the existing core nanoparticles, leading to the formation of a shell around the core. The pulses provide energy for the continued nucleation and growth process, facilitating the coating of core particles with the shell material. On the other hand, the sample prepared with 600 laser shots provided very well-defined spherical shapes with higher concentration and shell thickness (23.87nm) and a high agglomeration rate. This aggregation are strongly due to the electrostatic attractive force between nanoparticles produced by the electric double layer on the nanoparticles' surfaces. The nanoparticles are charged in liquid. An electrical layer surrounds the surface of the nanoparticles as a result of the interaction between the liquid molecules and the surface-charged nanoparticles. It is worth mentioning that interaction between the plasma plume and nanoparticles can take place, which depends on the attractive and repulsive forces between the plume species and nanoparticles. These forces, such as the attractive Van der Waals force, may cause growth and/or aggregation [55].

In summary, the number of laser pulses is a critical parameter in the laser ablation in liquid (PLAL) technique for forming core-shell nanoparticles. It influences the nucleation and growth phases, shell thickness, uniformity, composition, and application-specific properties. By carefully optimizing the number of pulses, researchers can tailor the core-shell nanoparticles' characteristics to meet specific application requirements, ensuring their effectiveness and reliability in various technological fields.

Finally, we have successfully fabricated core-shell nanoparticles as clearly by double SPR peaks in UV-Vis absorption spectra (355 and 526 nm which is a typical value for Au@ Nb_2O_5 NPs of this size) and supported by TEM images. These results are consistent with [56].

As shown in Table 4, the core size and shell thickness indicated that the shell thickness increased with the number of laser pulses, aligning with other reported studies [57, 58].

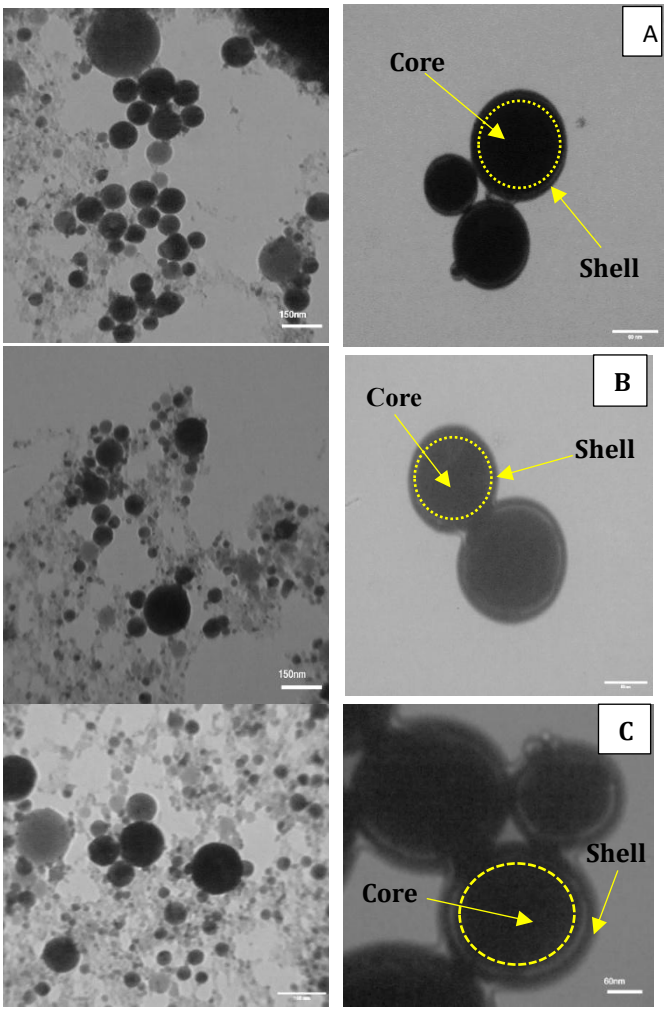

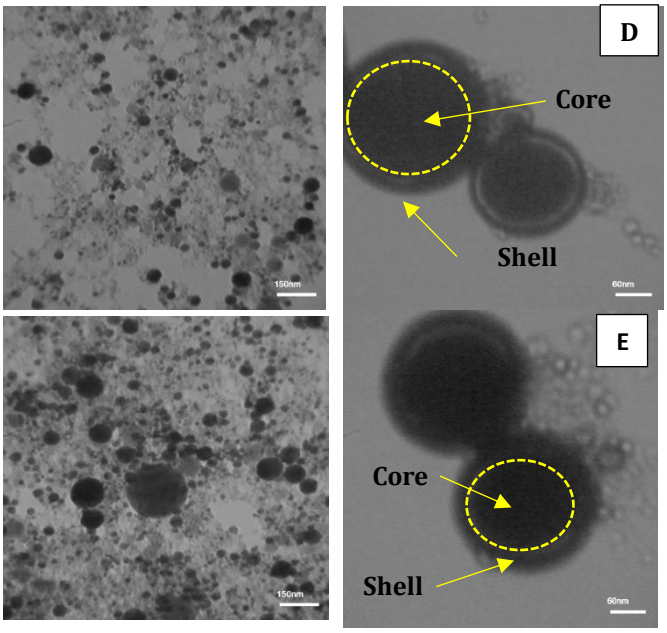

Figure 7. TEM images of Au@Nb_2O_5 NPs fabricated with varying laser shots: A: 200 pulses, B: 300 pulses, C: 400 pulses, D: 500 pulses, E: 600 pulses.

Table 4. Average dimensions of the core and shell thickness of Au@Nb_2O_5 nanoparticles

Number of laser pulses	Core size(nm)	Shell thickness(nm)
200	38.18	5.12
300	45.09	8.73
400	57.85	11.28
500	53.58	18.31
600	118. 1	23.87

3.5 Electrical Measurements of Au@Nb_2O_5 Thin Films'

The properties of hybrid materials, both thick and thin films, are being continuously studied. Core-shell materials containing niobium pentoxide are receiving increasing attention due to their potential uses in photovoltaic devices, such as heterojunction solar cells and photodetectors, as well as, gas sensing, and catalysts [59-62]. Attempts have also been made to fabricate stable and high-performance photodetectors from these materials [54].

The electrical resistivity of the Au@Nb_2O_5 films, prepared at a laser fluence of 127.3 J/cm^2, was evaluated over a wide temperature range (25-225 °C) to examine its semiconducting properties concerning the number of laser pulses (200, 300, 400, 500, and 600).

Temperature-dependent resistivity of the thin films was studied as a function of temperature (T). The results are shown in Figure 8. The resistivity values of Au@Nb_2O_5 thin films were high at low temperatures and then gradually decreased with increasing temperature. This phenomenon is characteristic of semiconductor materials, which exhibit a negative temperature coefficient, meaning that their resistivity decreases with increasing temperature. The initial evaluation of all samples was performed under thermal equilibrium conditions (at room temperature) to determine the resistivity of Au@Nb_2O_5 thin films prepared using various laser pulse parameters. The lowest resistivity was documented at about 9.75 kΩ. Figure 8 displays the resistivity values of the thin films as a function of increasing temperature.

The Au@Nb_2O_5 thin film, generated with 600 laser pulses, exhibited elevated resistance due to the influence of particle size, hopping mechanism, structural flaws, and film thickness on resistance values[63].

The resistivity's dependence on the number of laser pulses indicates an increase in resistivity with a higher number of pulses. This phenomenon can be elucidated by the conduction mechanism in Au@Nb_2O_5 thin films, which is thought to be associated with the concentration of electrical carriers, specifically the oxygen vacancies within the structure. The electrical properties of Au@Nb_2O_5 thin films are intrinsically linked to their microstructure and composition [64].

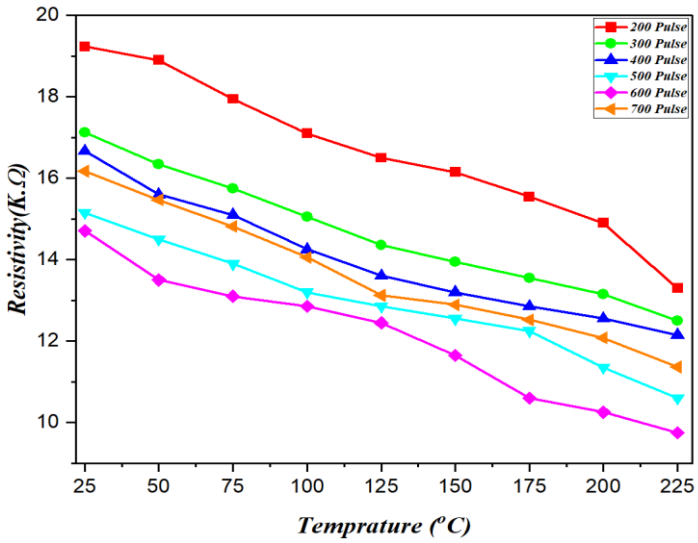

Figure 8. The resistivity for Au@Nb_2O_5 thin films as a function of the measurement temperature.

Nb_2O_5 nanoparticles have elevated light transmittance owing to their tunable bandgap (~2.5-3 eV), making them suitable for the detection of wavelengths in the visible and ultraviolet spectrum. The use of gold nanoparticles enhances light absorption via the surface plasmon resonance (SPR) phenomenon, hence improving the effectiveness of photodetectors[65, 66]. Nb_2O_5 may serve as a hole-conducting layer (HTL) in organic (perovskite) solar cells owing to its exceptional thermal stability and favorable conductivity[67, 68]. Gold nanoparticles increase light scattering inside the cell, extending the photon trajectory and promoting current production[69-71]. Nb_2O_5 is an efficient material for the detection of harmful gases (such as NO_2 and CO) owing to its nanoporosity and capacity to interact with gas molecules Nb_2O_5 is an efficient material for the detection of harmful gases (such as NO_2 and CO) owing to its nanoporosity and capacity to interact with gas molecules. The use of gold particles enhances sensing sensitivity by augmenting the quantity of catalytic sites on the surface[72-74].

4. CONCLUSION

The number of laser pulses during laser ablation in liquid (LAL) significantly influences the production and properties of core-shell nanoparticles. This method employs laser pulses to ablate a target substance in a liquid environment, resulting in the creation of nanoparticles. The optical, structural, topographical, morphological, and electrical analyses of Au@Nb_2O_5 demonstrated a comprehensive enhancement. X-ray diffraction (XRD) examination verified the development of the orthorhombic (T-Nb_2O_5) phase and the synthesis of Au nanoparticles. The transmission electron microscope photos reveal that the nanoparticles possess a spherical morphology, with shell thickness augmenting in correlation with the number of pulses, attributable to the heightened quantity of particles extracted from the target, so affirming the successful synthesis of nanoparticles. The existence of Au@Nb_2O_5 core-shell nanoparticles was confirmed using the XRD profile, which displayed distinct diffraction planes. The UV-visible spectra exhibited clear absorption peaks ranging from 350 to 520 nm, ascribed to the surface plasmon resonance of Au nanoparticles within the Nb_2O_5 matrix. The absorption of Au@Nb_2O_5 core-shell nanoparticles was seen to rise with the number of laser pulses, resulting in elevated absorbance values and a little redshift ascribed to particle size. The resistivity diminishes with an increasing number of pulses.

ACKNOWLEDGMENTS

The authors would like to thank the University of Anbar and the University of Technology-Iraq for the logistic support of this work.

REFERENCE

[1] X. Xu, L. Gao, and G. J. M. Duan, "The fabrication of Au@ C core/shell nanoparticles by laser ablation in solutions and their enhancements to a gas sensor," vol. 9, no. 6, p. 278, 2018.

[2] G. Tan *et al.*, "Freestanding three-dimensional core–shell nanoarrays for lithium-ion battery anodes," vol. 7, no. 1, pp. 1-10, 2016.

[3] H. Zhu *et al.*, "When cubic cobalt sulfide meets layered molybdenum disulfide: a core–shell system toward synergetic electrocatalytic water splitting," vol. 27, no. 32, pp. 4752-4759, 2015.

[4] Fakhri M. A.; Salim E. T.; Wahid M. H. A.; Salim Z. T.; Hashim U., A novel parameter effects on optical properties of the LiNbO3 films using sol-gel method, AIP Conference Proceedings, 2213, 20242 (2020) 10.1063/5.0000206

[5] J.-F. Li, Y.-J. Zhang, S.-Y. Ding, R. Panneerselvam, and Z.-Q. J. C. r. Tian, "Core–shell nanoparticle-enhanced Raman spectroscopy," vol. 117, no. 7, pp. 5002-5069, 2017.

[6] R. A. Rani, A. S. Zoolfakar, A. P. O'Mullane, M. W. Austin, and K. J. J. o. M. C. A. Kalantar-Zadeh, "Thin films and nanostructures of niobium pentoxide: fundamental properties, synthesis methods and applications," vol. 2, no. 38, pp. 15683-15703, 2014.

[7] H.-C. Lu, "Synthesis and electrochromic properties of niobium oxide nanocrystals," 2022.

[8] Alsultany F. H.; Alhasan S. F. H.; Salim E. T., Seed Layer-Assisted Chemical Bath Deposition of Cu2O Nanoparticles on ITO-Coated Glass Substrates with Tunable Morphology, Crystallinity, and Optical Properties, Journal of Inorganic and Organometallic Polymers and Materials, 31(9), 3749-3759 (2021) 10.1007/s10904-021-02016-y.

[9] I. Ahmad *et al.*, "A systematic review on Nb2O5-based photocatalysts: Crystallography, synthetic methods, design strategies, and photocatalytic mechanisms," vol. 324, p. 103093, 2024.

[10] A. Nikolov, I. Balchev, N. Nedyalkov, I. Kostadinov, D. Karashanova, and G. J. A. P. A. Atanasova, "Influence of the laser pulse repetition rate and scanning speed on the morphology of Ag nanostructures fabricated by pulsed laser ablation of solid target in water," vol. 123, pp. 1-11, 2017.

[11] S. Li, H. Zhang, L. Xu, and M. J. O. E. Chen, "Laser-induced construction of multi-branched CuS nanodendrites with excellent surface-enhanced Raman scattering spectroscopy in repeated applications," vol. 25, no. 14, pp. 16204-16213, 2017.

[12] Jehan A. Saimon, Suzan N. Madhat, Khawla S. Khashan, Azhar I. Hassan, Rana O. Mahdi, Rafah A. Nasif, Synthesis of CdxZn1-xO nanostructure films using pulsed laser deposition technique, AIP Conf. Proc. 2045, 020003 (2018) https://doi.org/10.1063/1.5080816.

[13] G. Garcia Guilen *et al.*, "Structure and morphologies of ZnO nanoparticles synthesized by pulsed laser ablation in liquid: Effects of temperature and energy fluence," vol. 162, pp. 561-570, 2015.

[14] N. Lasemi, U. Pacher, C. Rentenberger, O. Bomatí-Miguel, and W. J. C. Kautek, "Laser-assisted synthesis of colloidal Ni/NiOx core/shell nanoparticles in water and alcoholic solvents," vol. 18, no. 9, pp. 1118-1124, 2017.

[15] H. T. Halboos and E. T. Salim, "Silver doped niobium pentoxide nanostructured thin film, optical structural and morphological properties," in *IOP Conference Series: Materials Science and Engineering*, 2018, vol. 454, no. 1, p. 012174: IOP Publishing.

[16] Fakhri M. A.; Abdulwahhab A. W.; Dawood M. A.; Raheema A. Q.; Numan N. H.; Khalid F. G.; Wahid M. H. A.; Hashim U.; Salim E. T., Optical investigations of nano lithium niobate deposited by spray pyrolysis technique with injection of Li2CO3 and Nb2O5 as raw materials, International Journal of Nanoelectronics and Materials, 11(Special Issue BOND21), 103-108 (2018).

[17] A. E. Nogueira *et al.*, "CuO decoration controls Nb2O5 photocatalyst selectivity in CO2 reduction," vol. 3, no. 8, pp. 7629-7636, 2020.

[18] M. Ahmad *et al.*, "Phytogenic fabrication of ZnO and gold decorated ZnO nanoparticles for photocatalytic degradation of Rhodamine B," vol. 9, no. 1, p. 104725, 2021.

[19] E. Tunkara, *Indium Tin Oxide and Gold Nanoparticles for Use as a Spectral Filter in Concentrating Photovoltaic Thermal Systems*. The University of Tulsa, 2018.

[20] Fakhri M. A.; Bader B. A.; Khalid F. G.; Numan N. H.; Abdulwahhab A. W.; Hashim U.; Salim E. T.; Munshid M. A.; Salim Z. T., Optical and morphological studies of LiNbO3 nano and micro photonic structural, AIP Conference Proceedings, 2045, 20017 (2018) 10.1063/1.5080830.

[21] G. S. Jaber, K. S. Khashan, and M. J. Abbas, "Preparation ZnO nanoparticles with different concentration by laser ablation in liquid," *Eng. Technol. J,* vol. 39, pp. 197-202, 2021.

[22] I. Fratoddi, I. Venditti, C. Battocchio, G. Polzonetti, C. Cametti, and M. V. Russo, "Core shell hybrids based on noble metal nanoparticles and conjugated polymers: synthesis and characterization," *Nanoscale research letters,* vol. 6, pp. 1-8, 2011.

[23] R. Zamiri *et al.*, "Laser assisted fabrication of ZnO/Ag and ZnO/Au core/shell nanocomposites," *Applied Physics A,* vol. 111, pp. 487-493, 2013.

[24] Muhsien M. A.; Salem E. T.; Agool I. R.; Hamdan H. H., Gas sensing of Au/n-SnO2/p-PSi/c-Si heterojunction devices prepared by rapid thermal oxidation, Applied Nanoscience (Switzerland), 4(6), 719-732 (2014) 10.1007/s13204-013-0244-7.

[25] Fakhri M. A.; Wahid M. H. A.; Badr B. A.; Kadhim S. M.; Salim E. T.; Hashim U.; Salim Z. T., Enhancement of Lithium Niobate nanophotonic structures via spin-coating technique for optical waveguides application, EPJ Web of Conferences, 162, 1004 (2017) 10.1051/epjconf/201716201004.

[28] E. T. Salim, J. A. Saimon, M. K. Abood, M. A. Fakhri"Effect of silicon substrate type on Nb2O5/Si device performance: an answer depends on physical analysis," *Opt Quant Electron* **52**, 463 (2020). https://doi.org/10.1007/s11082-020-02588-y.

[29] M. Kovendhan *et al.*, "Spray deposited Nb 2 O 5 thin film electrodes for fabrication of dye sensitized solar cells," *Transactions of the Indian Institute of Metals,* vol. 64, pp. 185-188, 2011.

[30] C. D. Sai and A. B. Ngac, "Effect of core-shell structure on optical properties of Au-Cu2O nanoparticles," *Physica B: Condensed Matter,* vol. 532, pp. 216-220, 2018.

[31] Tawfiq Z. H.; Fakhri M. A.; Adnan S. A., Photonic Crystal Fibres PCF for Different Sensors in Review, IOP Conference Series: Materials Science and Engineering, 454(1), 12173 (2018) 10.1088/1757-899X/454/1/012173.

[32] E. T. Salim *et al.*, "The impact of laser pulses on the optical and structural characteristics of WO3 nanoparticles fabricated via laser ablation in liquid (PLAL)," *Journal of Optics,* pp. 1-15, 2024.

[33] L. C. Oliveira, H. S. Oliveira, G. Mayrink, H. S. Mansur, A. A. Mansur, and R. L. Moreira, "One-pot synthesis of CdS@ Nb2O5 core–shell nanostructures with enhanced photocatalytic activity," *Applied Catalysis B: Environmental,* vol. 152, pp. 403-412, 2014.

[34] N. Kumari *et al.*, "Dependence of photoactivity of niobium pentoxide (Nb2O5) on crystalline phase and electrokinetic potential of the hydrocolloid," *Solar Energy Materials and Solar Cells,* vol. 208, p. 110408, 2020.

[35] Roaa A. Abbas, Evan T. Salim & Rana O. Mahdi, Morphology transformation of Cu2O thin film: different environmental temperatures employing chemical method, J Mater Sci: Mater Electron 35, 1057 (2024). https://doi.org/10.1007/s10854-024-12823-x.

[36] C. Senthilkumar, "Synthesis and characterization of niobium doped titanium oxide for spintronics applications," *Nano-Structures & Nano-Objects,* vol. 35, p. 101021, 2023.

[37] S. S. Shaker, A. Mohammed, M. S. J. E. Khalaf, and T. Journal, "Effect of Laser Pulses on Characterization of Zincoxide Thin Film Prepared by PLD," vol. 36, no. 1 Part B, 2018.

[38] S. S. Shaker, A. Mohammed, and M. S. Khalaf, "Effect of Laser Pulses on Characterization of Zincoxide Thin Film Prepared by PLD," *Engineering and Technology Journal,* vol. 36, no. 1 Part B, 2018.

[39] Doaa A. Mahmoud, Evan T. Salim, Rana O. Mahdi, A. Mindil, Subash C. B. Gopinath & Motahher A. Qaeed, Laser Ablation of Tungsten Metal for Au@WO3 Core-Shell Formation: A Characterizing Study at Different Laser Fluences, Plasmonics (2024). https://doi.org/10.1007/s11468-024-02607-8

[40] J. Bai, J. Xue, R. Wang, Z. Zhang, and S. Qiu, "Synthesis of novel Au@ Void@ Nb 2 O 5 core–shell nanocomposites with enhanced photocatalytic activity," *Dalton Transactions,* vol. 47, no. 10, pp. 3400-3407, 2018.

[41] Y. Kamlag, A. Goossens, I. Colbeck, and J. Schoonman, "Laser CVD of cubic SiC nanocrystals," *Applied surface science,* vol. 184, no. 1-4, pp. 118-122, 2001.

[42] Fakhri M. A.; Numan N. H.; Mohammed Q. Q.; Abdulla M. S.; Hassan O. S.; Abduljabar S. A.; Ahmed A. A., Responsivity and response time of nano silver oxide on silicon heterojunction detector, International Journal of Nanoelectronics and Materials, 11(Special Issue BOND21), 109-114 (2018).

[43] M. M. Mahdi, A. M. Ali, M. A. Alalousi, D. A. Kadhim, and M. A. J. V. Abid, "Developing a copper-zinc-aluminum alloying technique by vacuum thermal deposition after irradiation by gamma rays (NaI (Ti)) with stabilized zinc metal," vol. 219, p. 112676, 2024.

[44] Azzam Y. Kudhur, Evan T. Salim, Ilker Kara, Makram A. Fakhri & Rana O. Mahdi, Structural optical and morphological properties of copper oxide nanoparticles ablated using pulsed laser ablation in liquid, J Opt 53, 1936–1945 (2024). https://doi.org/10.1007/s12596-023-01331-6.

[45] O. Milkovič, J. Michaliková, J. Bednarčík, and Š. Michalik, "Influence of nanoparticle size on strain at the core-shell interface," *Key Engineering Materials,* vol. 662, pp. 217-220, 2015.

[46] S. Heidarinassab, A. Nyabadza, I. U. Ahad, and D. Brabazon, "Investigation of ablation efficiency and properties of silicon carbide nanoparticles synthesised using pulsed laser ablation in liquid," *Optics and Lasers in Engineering,* vol. 180, p. 108341, 2024.

[47] A. Al-Hamaoy *et al.*, "Liquid Phase–Pulsed Laser Ablation: A route to fabricate different carbon nanostructures," *Applied Surface Science,* vol. 302, pp. 141-144, 2014.

[48] Zainab T. Hussain, Khawla S. Khashan, Rana O. Mahdi, Characterization of cadmium oxide nanoparticles prepared through Nd:YAG laser ablation process, Materials Today: ProceedingsVolume 42, Pages 2645 – 26482021. https://doi.org/10.1016/j.matpr.2020.12.594.

[49] M. M. A. Al-Mousawi, A. Al-Nafiey, and G. Al-Dahesh, "Studying the effect of the number of laser pulses on the structure, morphology, and optical properties for a thin film of GO-Ag nanocomposites," in *Journal of Physics: Conference Series*, 2021, vol. 1999, no. 1, p. 012141: IOP Publishing.

[50] P. Shanmugam, R. Rathanasamy, G. V. Kaliyannan, S. Sivaraj, M. Chinnasamy, and M. S. J. M. S. Anbupalani, "Performance enhancement of polycrystalline silicon solar cell through sputter coated molybdenum disulphide surface films," vol. 28, no. 2, pp. 157-163, 2022.

[51] G. Velu Kaliyannan, S. V. Palanisamy, R. Rathanasamy, M. Palanisamy, S. K. Palaniappan, and M. J. J. o. M. S. M. i. E. Chinnasamy, "Influence of ultrathin gahnite anti-reflection coating on the power conversion efficiency of polycrystalline silicon solar cell," vol. 31, pp. 2308-2319, 2020.

[52] Mohammed D.A.; Kadhim A.; Fakhri M.A., The enhancement of the corrosion protection of 304 stainless steel using Al2O3 films by PLD method, AIP Conference Proceedings, 2045, 20014 (2018) 10.1063/1.5080827.

[53] V. Vendamani, A. Tripathi, A. P. Pathak, S. V. Rao, and A. J. M. L. Tiwari, "Laser ablation of natural micas: synthesis of MgO and Mg (OH) 2 nanoparticles and nanochains," vol. 192, pp. 29-32, 2017.

[54] M. M. Mahdi, E. T. Salim, and A. S. J. P. Obaid, "A Comparison Study of Au@ Nb2O5 Core–Shell Nanoparticle Using Two Different Laser Flounces," pp. 1-14, 2025.

[55] D. Rosická and J. J. N. R. L. Šembera, "Changes in the nanoparticle aggregation rate due to the additional effect of electrostatic and magnetic forces on mass transport coefficients," vol. 8, pp. 1-9, 2013.

[56] Khawla S. Khashan, Aseel A. Hadi, Rana O. Mahdi & Doaa S. Jubair, Aluminum-doped zinc oxide nanoparticles prepared via nanosecond Nd: YAG laser ablation in water: optoelectronic properties, Opt Quant Electron 56, 125 (2024). https://doi.org/10.1007/s11082-023-05630-x.

[57] R. Riedel, N. Mahr, C. Yao, A. Wu, F. Yang, and N. J. N. Hampp, "Synthesis of gold–silica core–shell nanoparticles by pulsed laser ablation in liquid and their physico-chemical properties towards photothermal cancer therapy," vol. 12, no. 5, pp. 3007-3018, 2020.

[58] M. Siddiq *et al.*, "Synthesis of bimetallic core/shell nanoparticles via pulse laser ablation and their catalytic effectiveness in dye degradation," vol. 36, no. 3, 2024.

[59] B. Gao, J. Fu, K. Huo, W. Zhang, Y. Xie, and P. K. J. J. o. t. A. C. S. Chu, "Quasi-Aligned Ag–Nb2O5 Nanobelt Arrays with Enhanced Photocatalytic and Antibacterial Activities," vol. 94, no. 8, pp. 2330-2338, 2011.

[60] Rana O. Mahdi, Aseel A. Hadi, Juhaina M. Taha, Khawla S. Khashan, Preparation of nickel oxide nanoparticles prepared by laser ablation in water, AIP Conf. Proc. 2213, 020309 (2020) https://doi.org/10.1063/5.0000116.

[61] L.-W. Mao, L.-Y. Zhu, T. T. Wu, L. Xu, X.-H. Jin, and H.-L. J. A. S. S. Lu, "Excellent long-term stable H2S gas sensor based on Nb2O5/SnO2 core-shell heterostructure nanorods," vol. 602, p. 154339, 2022.

[62] X. Hu and H. J. F. o. O. Wang, "ZnO/Nb 2 O 5 core/shell nanorod array photoanode for dye-sensitized solar cells," vol. 11, pp. 285-290, 2018.

[63] G. Wisz, I. Virt, P. Sagan, P. Potera, and R. J. N. R. L. Yavorskyi, "Structural, optical and electrical properties of zinc oxide layers produced by pulsed laser deposition method," vol. 12, pp. 1-7, 2017.

[64] Hassen H. H.; Salim E. T.; Taha J. M.; Mahdi R. O.; Numan N. H.; Khalid F. G.; Fakhri M. A., Fourier transform infrared spectroscopy and photo luminance results for Zno NPs prepared at different preparation condition using LP-PLA technique, International Journal of Nanoelectronics and Materialsm, 11(Special Issue BOND21) 65-72 (2018).

[65] H.-L. Chen, Y.-M. Lu, and W.-S. J. M. t. Hwang, "Effect of film thickness on structural and electrical properties of sputter-deposited nickel oxide films," vol. 46, no. 4, pp. 872-879, 2005.

[66] Azzam Y. kudhur, Evan T. Salim, Ilker Kara, Rana O. Mahdi & Raed K. Ibrahim, The effect of laser energy on Cu2O nanoparticles formation by liquid-phase pulsed laser ablation, J Opt 53, 1309–1321 (2024). https://doi.org/10.1007/s12596-023-01319-2.

[67] J. Junesch, "Novel thin film nanohole devices for plasmonic sensing applications," ETH Zurich, 2015.

[68] Evan T. Salim, Ahmed T. Hassan, Rana O Mahdi, Forat H. Alsultany, Physical Properties of HfO2 Nano Structures Deposited using PLD, IJNeaM, vol. 16, no. 3, pp. 495–510, Oct. 2023.

[69] M. B. Coşar, "Tuning the electron beam evaporation parameters for the production of hole and electron transport layers for perovskite solar cells," Middle East Technical University (Turkey), 2019.

[70] Aseel A. Hadi, Juhaina M. Taha, Rana O. Mahdi, Khawla S. Khashan, Influence of laser pulse on properties of NiO NPs prepared by laser ablation in liquid, AIP Conf. Proc. 2213, 020308 (2020) https://doi.org/10.1063/5.0000115.

[71] N. Chander *et al.*, "Size and concentration effects of gold nanoparticles on optical and electrical properties of plasmonic dye sensitized solar cells," vol. 109, pp. 11-23, 2014.

[72] Khawla S khashan, Rana O Mahdi, Ban A. Badr, Farah Mahdi, Preparation and characterization of ZnMgO nanostructured materials as a photodetector, Journal of Physics: Conference Series 1795 (2021) 012008. doi:10.1088/1742-6596/1795/1/012008.

[73] R. A. Rani *et al.*, "Nanoporous Nb2O5 hydrogen gas sensor," vol. 176, pp. 149-156, 2013.

[74] Roaa A. Abbas, Evan T. Salim & Rana O. Mahdi, Deposition time effect on copper oxide nano structures, an analysis study using chemical method, J Mater Sci: Mater Electron 35, 427 (2024). https://doi.org/10.1007/s10854-024-12143-0.